Journal of Power Sources 217 (2012) 54–58

Contents lists available at SciVerse ScienceDirect

Journal of Power Sources

journal homepage: www.elsevier.com/locate/jpowsour

Short communication

LiF/Fe nanocomposite as a lithium-rich and high capacity conversion cathode material for Li-ion batteries

Ting Li*, Zhong X. Chen, Xin P. Ai, Yu L. Cao, Han X. Yang*

Department of Chemistry, Wuhan University, Wuhan 430072, China

HIGHLIGHTS

- The composite was prepared by a simple ball-milling of LiF and Fe powders.
- The composite delivers 568 mAh g^{-1} at 20 mA g^{-1} and exhibits a high rate capability.
- The composite can realize the conversion reaction of LiF/Fe to FeF_3 and vice versa.

ARTICLE INFO

Article history:
Received 22 February 2012
Received in revised form
25 May 2012
Accepted 29 May 2012
Available online 6 June 2012

Keywords:
Lithium fluoride
Iron
Electrochemical conversion reaction
High capacity cathode material
Lithium-ion battery

ABSTRACT

Lithium-rich LiF/Fe nanocomposite is prepared by a simple route of mechanical ball-milling of lithium fluoride and iron using rigid TiN nanoparticles as the grinding powders, and studied as a lithium-rich cathode material for satisfying the present Li-ion battery technology. The structural characterizations reveal that the nanocomposite is composed of well-dispersed and intimately contacted LiF and Fe particles created by high-energy ball-milling, forming appropriate electrode-active nanodomains for the reversible conversion reaction of LiF and Fe. Electrochemical measurements demonstrate that the LiF/Fe nanocomposite containing 50 wt% active materials of LiF and Fe can deliver a high reversible capacity of 568 mAh g^{-1} at 20 mA g^{-1} (calculated using the weight of LiF and Fe only), approaching the theoretical capacity of the composite (600 mAh g^{-1}), and also show a strong power capability with a reversible capacity of ~300 mAh g^{-1} even at a very high rate of 500 mA g^{-1} at room temperature. CV and XRD analyses confirm that the LiF/Fe nanocomposite can nearly realize a three-electron transfer through electrochemical conversion of LiF/Fe to FeF_3 and vice versa. These results suggest the possibility to utilize the inexpensive lithium-rich composites of lithium fluoride and metals as high-capacity cathode materials for future-generation Li-ion batteries through the electrochemical conversion.

1. Introduction

Li-ion batteries (LIBs) are now considered as a preferred power source for a variety of electric storage applications in the development of sustainable new energy technologies [1–3]. However, the most of LIB systems developed so far are based on transition metal oxide cathodes, which have severe cost and resource limitations that hinder their widespread electric storage applications. Moreover, these oxide cathodes store electric charges through lithium intercalation mechanism, which allows mostly no more than one-electron transfer per formula unit, thus limiting a full utilization of the oxidation states of the cathode materials [4,5]. Therefore, it is very desirable to develop alternative electric storage mechanisms using naturally abundant and low-cost cathode materials to enable high capacity Li-ion batteries for large scale applications.

Electrochemical conversion reaction offers an alternative reaction path to realize a large capacity charge storage of a transition-metal compound by complete utilization of its oxidation states [6–9]. In recent years, a vast array of metal fluorides [10–14], oxides [15–17], sulfides [18], and nitrides [19] have been demonstrated to produce a large multi-electron redox capacity through reversible electrochemical conversion reactions. Of these compounds, transition metal fluorides are being widely studied owing to their metallic cations in high oxidation states and a strong ionic character of M–F bonds, which are expected to give a high reversible capacity and high redox voltage [8,10]. Among metal fluorides, FeF_3 is particularly attractive as a potential cathode material because of its high theoretical three-electron redox capacity (712 mAh g^{-1}), low cost, and low toxicity [10,12,13].

* Corresponding authors. Tel.: +86 27 68754526; fax: +86 (0)27 87884476.
E-mail addresses: liting0828@163.com (T. Li), hxyang@whu.edu.cn (H.X. Yang).

0378-7753/$ – see front matter © 2012 Elsevier B.V. All rights reserved.
http://dx.doi.org/10.1016/j.jpowsour.2012.05.111

However, direct battery applications of FeF_3 cathode are difficult because present LIB technologies prefer to use lithium-deficient anodes, which require the corresponding cathodes to be in a lithium-rich state (discharged state) for the considerations of safety and convenience in production process. To solve this practical problem, an effective and simple way is to use a lithium-rich LiF/Fe composite that have the same chemical composition as the discharged state of FeF_3 cathode and can convert into FeF_3 at first charge, if the LiF and Fe phases are well dispersed and intimately contacted to form electrochemically active nanodomains [7,11,20,21]. As it is reported recently, a number of LiF/M (M = Ti, Co, Ni, Fe) nanocomposites prepared by pulse laser deposition or combinatorial cosputtering methods demonstrated a full electrochemical conversion from a discharged state to a charged state with lithium extraction, thus facilitating battery applications [21–24]. In addition, we also found that the well-mixed $Li_2O + CuO$ nanocomposite prefabricated by high-energy ball-milling can be reversibly cycled to $LiCuO_2$, liberating a lithium ion during the first charge as a lithium-rich conversion cathode in Li-ion configuration [25].

In the light of these reversal conversions of lithium-rich nanocomposites to their lithium-deficient high oxidation states, we prepared the LiF/Fe/C nanocomposites by high-energy ball-milling the electroactive components with rigid TiN nanoparticles, thus creating an electrochemically favorable structure with well-dispersed TiN/LiF + Fe/C nanodomains for cathodic conversion reaction. In this paper, we report the electrochemical behaviors of the nanocomposite as a conversion cathode and reveal the redox mechanism and structural evolution of the nanocomposite during the charge/discharge process.

2. Experimental

2.1. Materials preparation

The LiF/Fe/C nanocomposite was prepared by two-step mechanical ball-milling. Firstly, a stoichiometric mixture of lithium fluoride (LiF, 99.5%, Alfa-Aesar), reduced iron powder (99%), and nano-titanium nitride (TiN, 99.2%, ~20 nm, Hefei Kaier Nanomaterials Co., Ltd., China) was added to an argon-filled sealed stainless vessel and ball-milled using a high-energy mill (QM-3A, Nanjing, China) for 10 h. And then the as-obtained TiN/LiF + Fe nanocomposite was ball-milled with graphite (99% purity) using a planetary mill (QM-1SP04, Nanjing, China) with the rotation speed of 240 rpm for 10 h. The as-prepared TiN/LiF + Fe/C nanocomposite had a mass fraction of: Fe, 20.9%; LiF, 29.1%; TiN, 30%; graphite, 20%. The molar ratio of Fe to LiF in this composite was designed to be 1:3.

2.2. Structural characterization

The phase analysis of the ball-milled nanocomposite sample was performed using X-ray diffraction (XRD, Shimadzu XRD-6000) with Cu Kα radiation in a 2θ range from 10° to 80°. To characterize the structural changes at charged and discharged states, the electrode samples were taken out from the disassembled experimental cells and rinsed with pure dimethyl carbonate solvent in an Ar-filled glovebox and then immediately sent for ex-situ XRD analysis. The morphology and microstructure of as-prepared nanocomposite were observed using a high-resolution transmission electron microscopy (HRTEM, JEM-2100FEF). The samples for the HRTEM analysis were prepared by dispersing the sample powders in ethanol and releasing a few drops of the dispersed solution on a carbon film supported on a copper grid.

2.3. Electrochemical characterization

The LiF/Fe nanocomposite cathode was prepared by mixing 80 wt% nanocomposite, 10 wt% acetylene black, and 10 wt% polytetrafluoroethylene (PTFE) into ~0.1 mm thick film and pressing the cathode film onto an aluminum net. The charge–discharge experiments were carried out using coin cells (2032 type) which were assembled in an argon-filled glovebox with Li metal foil as the anode, a microporous membrane (Celgard 2400) as the separator and 1 mol L^{-1} solution of $LiPF_6$ dissolved in a mixed solvent of ethylene carbonate (EC), dimethyl carbonate (DMC), and ethylene methyl carbonate (EMC) (1:1:1 by wt) as the electrolyte. The cells were controlled by an automatic battery tester (Land CT2001A, Wuhan, China) between 4.5 V and 1.0 V at different current densities. Cyclic voltammograms (CV) were measured using an electrochemical station (CHI660a, Shanghai, China) by the three-electrode cell at a scanning rate of 0.1 mV s^{-1} in a voltage range of 4.5–1.0 V.

3. Results and discussion

3.1. Structural features

In order to overcome the poor conductivity and high lattice energy barrier of LiF and then to enhance the conversion activity of the phase transformation reaction, the LiF and Fe particles need to be downsized as small as possible and closely contacted as tight as possible to create sufficient electroactive interfaces for reversible structural conversion [7,20]. The preparation process of LiF/Fe/C nanocomposite in our work is schematically illustrated in Fig. 1. Firstly, the LiF and Fe powder was ground with rigid TiN nanoparticles to form uniformly dispersed and electrically wired TiN/LiF + Fe nanocomposite particles, where the TiN nanoparticles act not only as a grinding powder to pulverize the LiF + Fe mixture into nanosized particles but also as conductive nanocores to fix the electroactive components, preventing them from phase segregation and aggregation. After then, the nanocomposite was coated with graphite by planetary ball-milling to further ensure the electronic conduction in-between the particles and to prevent the nanoparticles from aggregating at cycling. Apparently, such a core-shell-like nanostructure with well-contacted phases confined in a nanodomain may be favorable for the phase transformation reaction, promoting the conversion reaction of LiF + Fe into a chargeable FeF_3 phase. Different mass fractions of LiF, Fe, TiN and graphite, and different ball-milling times were tested for the optimization of the preparation conditions. It was found that the composite material fabricated with a mass fraction of 50% Fe + LiF, 30% TiN, and 20% graphite, high-energy ball-milled for 10 h, and planetary ball-milled for 10 h had the smallest particle size and the best dispersion of the different phases, showing the best charge–discharge performances. Thus the composite material prepared in such condition is discussed below.

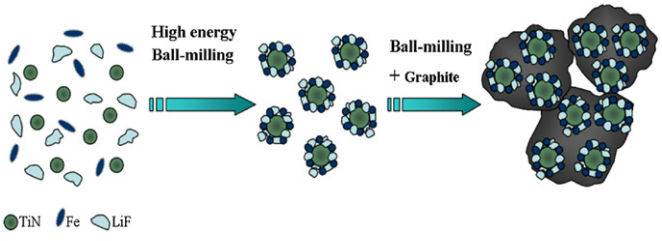

Fig. 1. Schematic illustration of the preparation process of the TiN/LiF + Fe/C nanocomposite.

To confirm the crystalline phases in the composite, XRD analysis was carried out for the LiF/Fe/C composite. As shown in Fig. 2, all the phases of LiF, Fe, TiN, and graphite are clearly observed without diffraction from impurities, suggesting no chemical reactions occurring in the electroactive components during the ball-milling. The XRD signals of LiF and Fe in the composite appeared to be weak and broad, implying a decrease in the crystallinity of the electrode-active particles after high-energy ball-milling. Unfortunately, the main peaks of Fe (44.7°) and LiF (45°) are closely located and partially overlapped, which adds a great uncertainty for calculating the average size of LiF and Fe particles from the Scherer equation.

The morphological features and particle sizes of the LiF/Fe composite can be clearly visualized from their TEM images as displayed in Fig. 3a. The composite appears as microsized grains aggregated with ~10 nm nanoparticles of LiF and Fe, which were downsized and uniformly mixed at nanoscale by high-energy ball-milling. As seen from the magnified HRTEM image on an edge part of a single particle (Fig. 3b), the darker areas dotted in inner part of the grain have a regular lattice fingerprint of $d = 0.212$ nm, corresponding to the (200) plane of cubic TiN (JCPDS No. 38-1420), and all the surrounding regions show a lattice fringe with a d-spacing of 0.203 nm, characteristic of the (110) plane of cubic Fe (JCPDS No. 06-0696). At the edge of the region, a clear lattice fringe appears, corresponding to the (002) plane ($d = 0.337$ nm) of hexagonal graphite (JCPDS No. 41-1487). The observations above indicate that the composite nanoparticles are uniformly coated by graphite, which may greatly enhance the conduction of the composite. The lattice fringe of LiF is hardly discerned in the image, possibly because its crystalline lattice was collapsed during the severe high-energy ball-milling. Nevertheless, the nanodomains formed in the composite with different phases well-dispersed and intimately contacted are no doubt favorable for the phase transformation reaction and also effective to prevent the electrode-active nanoparticles from aggregation.

3.2. Electrochemical performances

The conversion degree and reversibility of the LiF/Fe/C nanocomposite were evaluated by galvanostatic charge/discharge cycling at room temperature. Fig. 4 displays the voltage profiles of the LiF/Fe/C electrode cycled in the voltage region of 4.5–1.0 V at

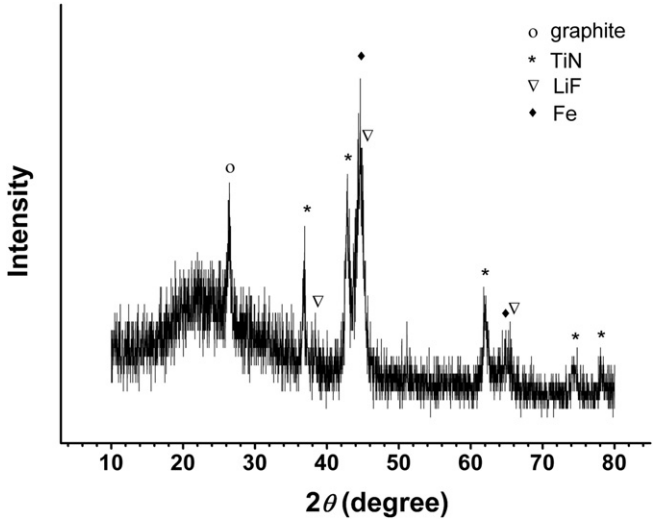

Fig. 2. XRD pattern of the as-prepared TiN/LiF + Fe/C nanocomposite.

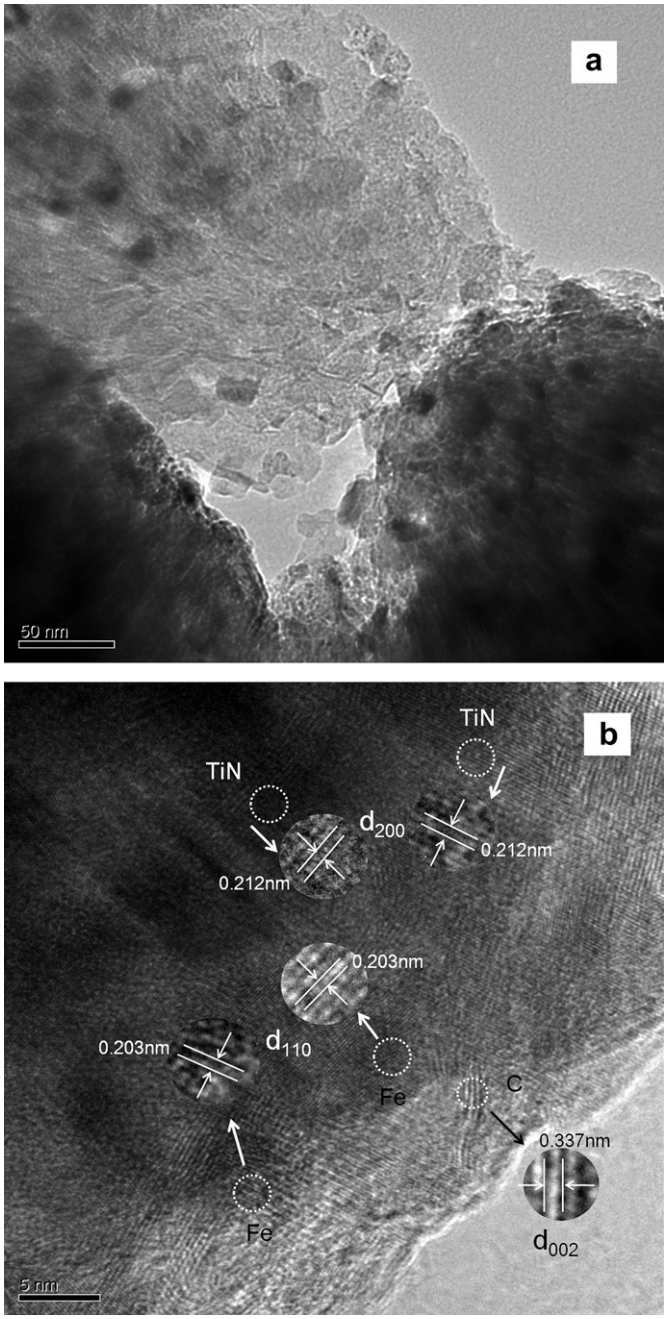

Fig. 3. (a) TEM image and (b) expanded TEM image of the TiN/LiF + Fe/C nanopowder.

a current density of 20 mA g^{-1}. At the first charge, the potential of the composite electrode climbed up from its open-circuit potential of +3.0 V to a high potential of +4.3 V and then remained steadily till a cutoff potential of +4.5 V, totally taking in a charge capacity of 389 mAh g^{-1}. During the subsequent discharge, the electrode showed a two-staged discharge profile with a sloping part at 3.3–2.3 V, followed with a lower voltage plateau at 2.3–1.6 V, very similar to the discharge curve of FeF_3 electrodes reported in recent publications [10,12]. Analogously, the observed two-staged discharge could be attributed to a one-electron reduction of Fe^{3+} to Fe^{2+} with Li^+ insertion and a successive two-electron reduction of Fe^{2+} to Fe^0 through the conversion reaction. The first step delivered a capacity of ~150 mAh g^{-1} and the second step gave a huge capacity of ~400 mAh g^{-1}. The excessive capacity below

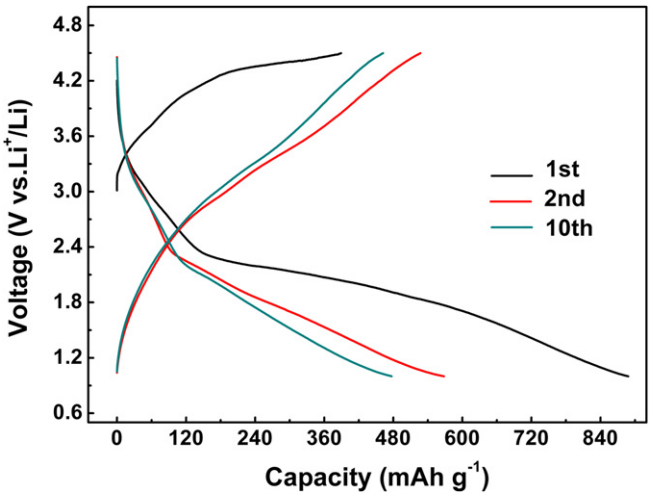

Fig. 4. Charge/discharge profiles of the LiF/Fe nanocomposite electrode at a constant current of 20 mA g^{-1} in the voltage region of 4.5–1.0 V.

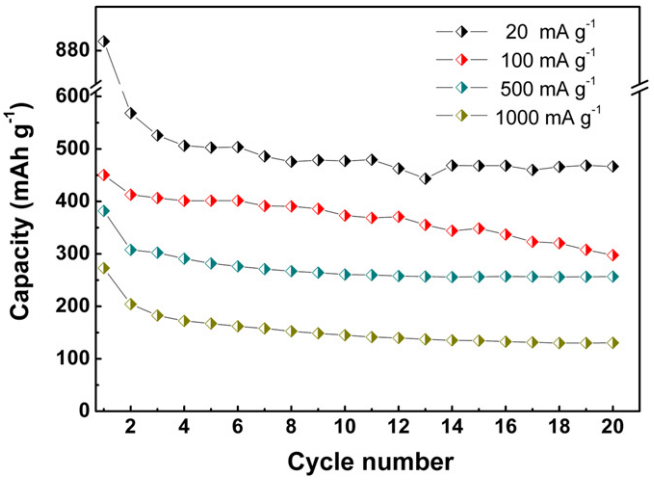

Fig. 5. Cycling performance of the LiF/Fe electrode at various current rates as labeled in the figure.

1.5 V may originate from an electrolyte decomposition at low potentials as discussed in relevant studies [26,27]. From the second cycle, the electrode displayed the two-stage voltage profiles with a charge and discharge capacity of 527 and 568 mAh g^{-1}, respectively, approaching to the theoretical capacity (600 mAh g^{-1}) as expected from a complete three-electron reaction of $3LiF + Fe \leftrightarrow FeF_3 + 3Li^+$. It should be mentioned that the high capacity delivered by LiF–Fe composite electrode in this study is calculated using the weight of LiF and Fe as the active materials, which is 50% of the total composite material. These stepwise charge–discharge profiles and near three-electron redox capacities suggest that the LiF/Fe nanocomposite prepared by simple high-energy ball-milling can be converted from Fe^0 to Fe^{3+} and vice versa, realizing a reversible 3-electron redox capacity, which is much higher than those prepared by combinatorial cosputtering or pyrolysis [24,28,29]. However, it should be mentioned that the nanocomposite electrode exhibited a smaller charging capacity than the corresponding discharge capacity at the first cycle, which leads to a doubtful high coulombic efficiency of >100%. This phenomenon may arise from two causes: first, there may exist some amount of high valent Fe in the composite brought about by the oxidation of Fe^0 particles in the duration of materials processing. Secondly, there may also exist a number of highly active surface groups and sites on the nanoparticles produced by high-energy ball-milling, which contribute extra irreversible capacity during the first discharge.

To test the reversibility and capacity retention of the LiF/Fe nanocomposite as a feasible cathode material, we cycled the electrode at different current rates at room temperature. Fig. 5 shows the cycling performance of the LiF/Fe/C electrode at various current densities. The composite electrode could keep a reversible capacity of 467 mAh g^{-1} after 20 cycles at a moderate current density of 20 mA g^{-1}. At a considerable high rate of 500 mA g^{-1}, the electrode can still deliver an initial discharge capacity of 382 mAh g^{-1} and remain ~300 mAh g^{-1} after 20 cycles. Even at a very high value of 1000 mA g^{-1}, the reversible discharge capacity could still reach ~200 mAh g^{-1} at cycling. This high-rate capability and cycling stability suggest that the electrochemical conversion reaction of the LiF/Fe nanocomposites could occur reversibly as long as the Fe and LiF particles are sufficiently downsized and uniformly dispersed so as to build up kinetically favorable interfaces that promote the phase-transformation reactions. Moreover, TiN nanoparticles as an inactive phase confined in the nanodomains can be effective to prevent the electrode-active nanoparticles from aggregation, improving cycleability of the LiF/Fe nanocomposite electrode.

3.3. Electrochemical conversion mechanism

In principle, the only difference in the conversion reactions of the LiF/Fe composite and the FeF_3 cathode is that the LiF/Fe composite needs to be converted to FeF_3 at first charge and then go through reversible electrochemical conversions in the same way as prefabricating FeF_3 cathode. To convince the effective conversion of the LiF/Fe composite into a FeF_3 phase, the cyclic voltammetric response (CV) of the composite electrode was measured using a three-electrode cell. Fig. 6 shows typical CV curves of the LiF/Fe electrode at a slow scan rate of 0.1 mV s^{-1} in a wide voltage range of 4.5–1.0 V. In the first positive scan, there were two weak oxidation peaks at 3.9 and 4.15 V, exclusively due to the two-step oxidation of Fe metal to form FeF_3 with participation of LiF. In the reversed scan, the first small reduction peak appeared at 3.0 V, followed by a broad band at 2.4–1.2 V, which resemble very much the CV features of FeF_3. Based on the conversion mechanism of FeF_3, the first reduction peak is likely brought about by Li^+ insertion into the

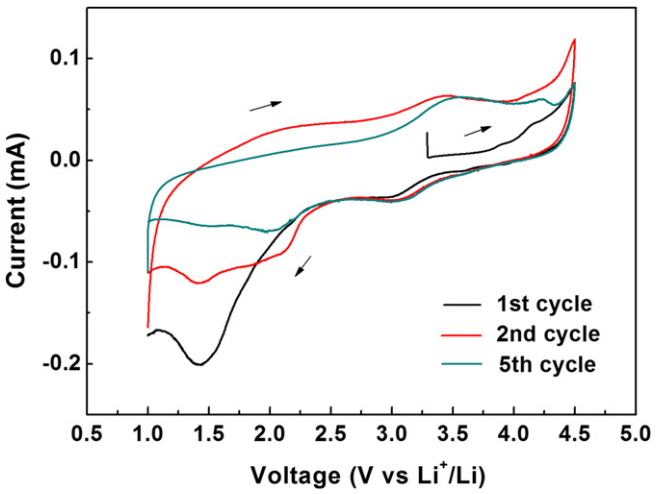

Fig. 6. Cyclic voltammograms of the LiF/Fe electrode in1 mol L^{-1} $LiPF_6$ + EC-DMC-EMC (1:1:1 by wt) solution. Scan rate: 0.1 mV s^{-1}.

FeF_3 to form $LiFeF_3$, and the second broad band is attributed to successive reductive decomposition of $LiFeF_3$ into LiF and Fe^0 [10,12,30]. In the second anodic scan, a broad band at 1.8–2.7 V and a small peak at 3.4 V appeared, which are reasonably attributed to the reverse oxidation reactions for the FeF_3 formation through two steps: electrochemical conversion of the LiF/Fe^0 nanomixture into a $LiFeF_3$ phase, and consecutive Li^+ deintercalation from the $LiFeF_3$ phase to regenerate FeF_3 nanocrystals. However, the reduction peak at the low voltage of ~1.4 V obviously decreased in the subsequent cathodic scan, indicating the reduction peak at this low voltage in the first negative scan should be attributed to the reductive decomposition of electrolyte occurred on the electrode surface, in accordance with the irreversible capacity of the LiF/Fe electrode at the initial discharge shown in Fig. 4. Thus, the overall charge–discharge reaction of the LiF/Fe electrode could be described as:

$$3\,LiF + Fe \leftrightarrow LiFeF_3 + 2\,Li^+ + 2e^- \quad (1)$$

$$LiFeF_3 \leftrightarrow FeF_3 + Li^+ + e^- \quad (2)$$

To further confirm the assignments of the CV features and related structural conversions, we carried out ex-situ XRD analysis of the LiF/Fe electrode discharged and charged in different depths. Since the ball-milled composite has very small size with low crystallinity, it is difficult to get an insight into the structural evolutions of the composite electrode in the duration of charge and discharge from XRD signals. However, the structural conversion of the electrode samples from a fully charged state to a discharged state is still discernible. As shown in Fig. 7, the XRD pattern of the LiF/Fe composite at open circuit well reflects the phases of LiF, Fe, TiN, and graphite. When fully charged to 4.5 V, the intensities of the LiF peak at 38.6° and the Fe peak at 44.7° decreased, revealing Fe and LiF were partially converted through the electrochemical conversion reaction. However, the main diffraction peak of FeF_3 phase which should emerge at 23.8° is too weak to be observed. This may be attributed to the low crystallinity of the FeF_3 phase in a nanosized and well-dispersed state, which is necessary for the conversion reaction. When the electrode was fully discharged to 1.0 V, the peaks of LiF and Fe obviously broadened and increased their intensities, suggesting the reversible conversion of FeF_3 to reproduce Fe metal and LiF. This reversible change in the XRD pattern of the electrode demonstrates the reversible structural conversion of the LiF/Fe nanocomposite between its initial discharged state and fully charged state.

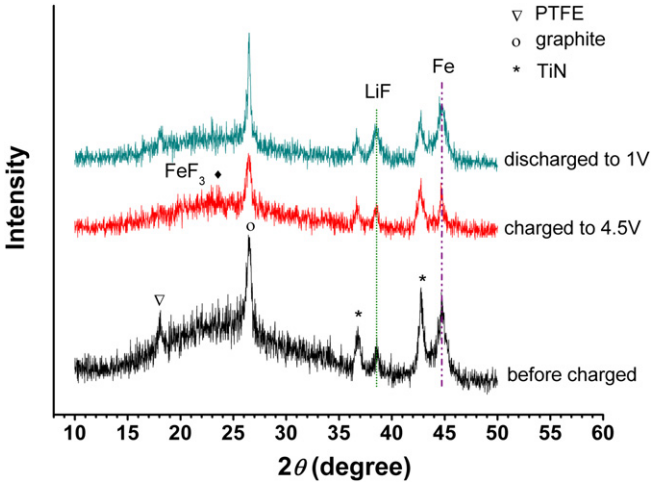

Fig. 7. Ex-situ XRD patterns of the LiF/Fe electrode at fully charged and discharged states as labeled in the figure.

4. Conclusions

In summary, we prepared LiF/Fe nanocomposite by high-energy ball-milling using conductive TiN nanoparticles as grinding powders and investigated this nanocomposite as a lithium-rich cathode material for Li-ion batteries. The as-prepared LiF/Fe nanocomposite with 50 wt% active materials of LiF and Fe can not only deliver a very high capacity of 568 mAh g^{-1} at 20 mA g^{-1} but also exhibit a high rate capability with a reversible capacity of ~300 mAh g^{-1} at 500 mA g^{-1} (the capacity is calculated using the weight of LiF and Fe only). The CV and XRD evidences demonstrated that the LiF/Fe nanocomposite electrode can realize a reversible electrochemical conversion reaction from Fe^0 to Fe^{3+} and vice versa, enabling a complete utilization of its three-electron redox capacity (600 mAh g^{-1}). These results reveal the possibility to realize a conversion reaction as long as lithium fluoride and metal particles are intimately contacted to form electrode-active nanodomains, and suggest a potential feasibility to use these nanocomposites as high capacity lithium-rich cathode materials for Li-ion batteries.

Acknowledgment

The authors acknowledge the financial support by the 973 Program, China (Grant No. 2009CB220103).

References

[1] J.M. Tarascon, M. Armand, Nature 414 (2001) 359.
[2] M. Armand, J.M. Tarascon, Nature 451 (2008) 652.
[3] B. Dunn, H. Kamath, J.M. Tarascon, Science 334 (2011) 928.
[4] M.S. Whittingham, Chem. Rev. 104 (2004) 4271.
[5] B.L. Ellis, K.T. Lee, L.F. Nazar, Chem. Mater 22 (2010) 691.
[6] X.P. Gao, H.X. Yang, Energy Environ. Sci. 3 (2010) 174.
[7] J. Cabana, L. Monconduit, D. Larcher, M.R. Palacín, Adv. Mater. 22 (2010) E170.
[8] H. Li, P. Balaya, J. Maier, J. Electrochem. Soc. 151 (2004) A1878.
[9] G.G. Amatucci, N. Pereira, J. Fluorine Chem. 128 (2007) 243.
[10] F. Badway, N. Pereira, F. Cosandey, G.G. Amatucci, J. Electrochem. Soc. 150 (2003) A1209.
[11] H. Li, G. Richter, J. Maier, Adv. Mater 15 (2003) 736.
[12] T. Li, L. Li, Y.L. Cao, X.P. Ai, H.X. Yang, J. Phys. Chem. C 114 (2010) 3190.
[13] S.W. Kim, D.H. Seo, H. Gwon, J. Kim, K. Kang, Adv. Mater 22 (2010) 5260.
[14] C.L. Li, L. Gu, S. Tsukimoto, P.A. van Aken, J. Maier, Adv. Mater 22 (2010) 3650.
[15] P. Poizot, S. Laruelle, S. Grugeon, L. Dupont, J.M. Tarascon, Nature 407 (2000) 496.
[16] P.L. Taberna, S. Mitra, P. Poizot, P. Simon, J.M. Tarascon, Nat. Mater. 5 (2006) 567.
[17] K.M. Shaju, F. Jiao, A. Debart, P.G. Bruce, Phys. Chem. Chem. Phys. 9 (2007) 1837.
[18] A. Débart, L. Dupont, R. Patrice, J.M. Tarascon, Solid State Sci. 8 (2006) 640.
[19] B. Das, M.V. Reddy, P. Malar, T. Osipowicz, G.V. Subba Rao, B.V.R. Chowdari, Solid State Ionics 180 (2009) 1061.
[20] P.G. Bruce, B. Scrosati, J.M. Tarascon, Angew. Chem., Int. Ed 47 (2008) 2930.
[21] X.Q. Yu, J.P. Sun, K. Tang, H. Li, X.J. Huang, L. Dupont, J. Maier, Phys. Chem. Chem. Phys. 11 (2009) 9497.
[22] Y.N. Zhou, W.Y. Liu, M.Z. Xue, L. Yu, C.L. Wu, X.J. Wu, Z.W. Fu, Electrochem. Solid-State Lett. 9 (2006) A147.
[23] Y.N. Zhou, C.L. Wu, H. Zhang, X.J. Wu, Z.W. Fu, Acta Phys. Chim. Sin. 22 (2006) 1111.
[24] P. Liao, B.L. MacDonald, R.A. Dunlap, J.R. Dahn, Chem. Mater. 20 (2008) 454.
[25] T. Li, X.P. Ai, H.X. Yang, J. Phys. Chem. C 115 (2011) 6167.
[26] A.J. Gmitter, F. Badway, S. Rangan, R.A. Bartynski, A. Halajko, N. Pereira, G.G. Amatuccia, J. Mater. Chem. 20 (2010) 4149.
[27] A. Ponrouch, P.-L. Taberna, P. Simon, M.R. Palacín, Electrochim. Acta 61 (2012) 13.
[28] R. Prakash, A.K. Mishra, A. Roth, C. Kübel, T. Scherer, M. Ghafari, H. Hahn, M. Fichtner, J. Mater. Chem. 20 (2010) 1871.
[29] R. Prakash, C. Wall, A.K. Mishra, C. Kübel, M. Ghafari, H. Hahn, M. Fichtner, J. Power Sources 196 (2011) 5936.
[30] N. Yamakawa, M. Jiang, B. Key, C.P. Grey, J. Am. Chem. Soc. 131 (2009) 10525.